



Preparation of photo-crosslinked hyaluronic acid/silk fibroin hydrogel for promoting wound healing

Shujing Li^{1,2,3,4} , Wensheng Pan^{2,3,4*} , Maohu Chen^{1,2,3,4} , Ruyue Wang^{1,2,3,4} , Feng Chen^{1*} 

¹Institute of Polymer Materials and Engineering, College of Materials Science and Engineering, Zhejiang University of Technology, Hangzhou 310014, Zhejiang, P. R. China

²Department of Gastroenterology, Zhejiang Provincial People's Hospital, Affiliated People's Hospital, Hangzhou Medical College, Hangzhou 310014, Zhejiang, P. R. China

³Institute of Gastrointestinal Diseases, Hangzhou Medical College, Hangzhou 310014, Zhejiang, P. R. China

⁴Zhejiang Provincial Engineering Laboratory of Diagnosis, Treatment and Pharmaceutical Development of Gastrointestinal Tract Tumors, Hangzhou 310014, Zhejiang, P. R. China

***Correspondence:** Wensheng Pan, Department of Gastroenterology, Zhejiang Provincial People's Hospital, Affiliated People's Hospital, Hangzhou Medical College, Hangzhou 310014, Zhejiang, P. R. China. wspan223@163.com; Feng Chen, Institute of Polymer Materials and Engineering, College of Materials Science and Engineering, Zhejiang University of Technology, Hangzhou 310014, Zhejiang, P. R. China. chenf@zjut.edu.cn

Academic Editor: Maryam Tabrizian, McGill University, Canada

Received: November 30, 2024 **Accepted:** April 25, 2025 **Published:** May 22, 2025

Cite this article: Li S, Pan W, Chen M, Wang R, Chen F. Preparation of photo-crosslinked hyaluronic acid/silk fibroin hydrogel for promoting wound healing. *Explor BioMat-X*. 2025;2:101339. <https://doi.org/10.37349/ebmx.2025.101339>

Abstract

Aim: Acute cutaneous injuries and refractory chronic wounds represent prevalent clinical challenges in daily life. To address the impediments to wound healing, we propose a novel hydrogel-based therapeutic approach designed to prevent bacterial invasion, mitigate infection-induced persistent inflammatory responses, and reduce excessive oxidative stress, thereby enhancing the wound healing process.

Methods: This study presents a method for preparing hyaluronic acid/silk fibroin (HA/SF) composite hydrogels via photo-crosslinking. HA and SF were respectively modified via methacrylation and glycidyl methacrylate to synthesize HAMA and SFMA. Mussel-inspired catechol groups were then grafted onto HAMA chain segments to prepare precursor HAC. Under photo-initiator LAP, polymerization was triggered to ultimately form a hydrogel network integrating mechanical toughness and tissue adhesiveness. Composite hydrogels with varying degrees of crosslinking are synthesized by adjusting the SFMA content.

Results: The results demonstrate that this hydrogel can effectively achieve hemostasis within 20 seconds. Lap shear testing revealed that the HASF-gel-2 hydrogel exhibited the highest maximum adhesive strength of 160.3 kPa among all experimental groups. Furthermore, while the cell viability of the control group was normalized to 1, the composite hydrogel groups displayed values of 1.015, 1.085, 1.136, and 1.263, respectively, indicating favorable biocompatibility. The appropriate incorporation of SF was shown to enhance cellular proliferation. On day 3 post-wounding, the HASF hydrogel group demonstrated a wound closure rate of 41.7%, outperforming commercial products under identical conditions.

Conclusions: In rat wound models, the HASF composite hydrogel significantly accelerated wound healing progression.



Keywords

Photo-crosslinking, hyaluronic acid, silk fibroin, hemostatic repair, wound dressing

Introduction

The skin is a vital immune organ of the human body, effectively preventing microbial invasion [1, 2]. However, factors such as infection [3], excessive inflammation, and complications can significantly hinder or delay this process, leading to chronic wounds. Once skin is damaged by external factors, the wound healing process is initiated. Bacterial infections can delay wound healing and cause the wound to deteriorate. Microbial infections [4] associated with skin injuries remain one of the most serious clinical problems, significantly impacting patients' quality of life and health. In recent years, various hydrogels have been developed as wound dressings, yet there is still a strong need for the design of photothermal composite hydrogels with both antibacterial and antioxidant properties to accelerate the healing of infected wounds.

Wound healing occurs in four distinct but interconnected stages [5–8]: hemostasis, inflammation, proliferation, and remodeling. However, traditional wound dressings typically support only one or two of these stages, which may severely compromise the overall healing process. Conventional wound dressings such as non-woven fabrics [9], bandages, and sponges [10] are often insufficient in protecting the wound and promoting healing. In contrast, hydrogels [11–14], highly hydrophilic polymers with high water content, biocompatibility, and flexibility, have emerged as promising materials for wound care. The network structure of hydrogels allows for effective absorption of excess wound exudate, creating an optimal healing environment. Additionally, hydrogels can be shaped to suit different wound types, providing good adhesion, antibacterial properties, and versatility, which has led to their widespread use in biomedical applications.

Hyaluronic acid (HA) [15–17] is a linear anionic polysaccharide composed of repeating disaccharide units of D-glucuronic acid and *N*-acetyl-D-glucosamine, connected alternately by β -1,3-glycosidic and β -1,4-glycosidic bonds. It is a major component of the extracellular matrix and is widely distributed in tissues such as the skin, synovial fluid, and vitreous body. In addition to its excellent biocompatibility, HA possesses good water solubility, wide availability, and low cost. It also plays a critical role in various physiological processes, including cell signal transduction, migration, and proliferation. By promoting skin hydration and controlling inflammation, HA plays a crucial role in wound healing. Furthermore, HA can promote angiogenesis by modulating the inflammatory response, thereby aiding wound healing. Given these properties, HA is an ideal candidate for hydrogel-based wound dressings. The hydroxyl and carboxyl groups in HA are easily modified to introduce various functional groups, such as mercaptan, aldehyde, or dihydrazide, which can be crosslinked to form hydrogels.

Silk fibroin (SF) [18, 19], derived from silkworms, is another natural biopolymer widely used in wound dressings, cell culture, tissue engineering, and other biomedical applications due to its excellent mechanical strength and biological activity. Furthermore, UV crosslinking is a chemical crosslinking technique known for its in-situ gelation capability, meaning that crosslinking occurs during the formation process without additional chemical treatment. This method allows precise control over the shape of the hydrogel, whether round, square, or complex shapes, and has the advantage of mild reaction conditions and short curing times, which is ideal for rapid prototyping or immediate applications. However, the mechanical and adhesive strength of single-phase HA hydrogels is often insufficient for wound repair. To address this limitation, combining HA with SF to create composite hydrogels can leverage the advantages of both materials, achieving a synergistic effect.

In this study, a novel hydrogel wound dressing was developed that can be rapidly photo-crosslinked using HA and SF. First, the hydroxyl group of HA was esterified with methacrylate anhydride (MA) to produce methacrylated hyaluronic acid (HAMA). HAMA was then modified with dopamine hydrochloride to introduce catechol groups, resulting in HAC. Meanwhile, SF was modified with glycidyl methacrylate (GMA)

via amidation to yield SFMA. The amidated SFMA and HAC were mixed in an aqueous solution containing the photo-initiator LAP. Finally, UV light was used to initiate the photo-crosslinking of HAC/SFMA (HASF), forming HASF hydrogels.

By varying the content of SFMA, hydrogels with different crosslinking degrees were obtained, and the effects of crosslinking on the internal microstructure, mechanical properties, swelling, degradation, and biocompatibility of HASF hydrogels were systematically evaluated. Animal studies further confirmed the efficacy of HASF hydrogels in hemostasis and wound treatment, making them a promising material for future wound care applications.

Materials and methods

Materials

Sodium hyaluronate (Mn = 100,000, 99%), Liyang Biotechnology Co., Ltd.; cicada cocoon, Hangzhou Jiuyuan Silk Culture Co., Ltd.; 50WX8100-200(H) ion exchange resin (99%), Titan Technology; anhydrous ethanol (AR), Sinopharm Group Chemical Reagent Co., Ltd.; sodium chloride (AR), Sinopharm Chemical Reagent Co., Ltd.; sodium hydroxide (AR), Sinopharm Chemical Reagent Co., Ltd.; *N,N*-dimethylformamide (AR), Sinopharm Chemical Reagent Co., Ltd.; dopamine hydrochloride (98%), Aladdin Reagent (Shanghai) Co.; tetrabutyl ammonium hydroxide aqueous solution (AR), Sinopharm Chemical Reagent Co., Ltd.; concentrated hydrochloric acid (37%), Sinopharm Chemical Reagent Co., Ltd.; methacrylic anhydride (AR), Aladdin Reagent (Shanghai) Co.; glycidyl methacrylate (AR), Aladdin Reagent (Shanghai) Co.; LAP photo-initiator (98%), Aladdin Reagent (Shanghai) Co.; 1-hydroxybenzotriazole hydrate (99%), Sinopharm Chemical Reagent Co., Ltd.; anhydrous sodium carbonate (99%), McLean Reagent (Shanghai) Co.; hyaluronidase (AR), Aladdin Reagent (Shanghai) Co.; *N,N*-diisopropyl carbodiimide (98%), Sinopharm Chemical Reagent Co., Ltd.; 4-dimethylaminopyridine (99%), Aladdin Reagent (Shanghai) Co.; 1-hydroxybenzotriazole monohydrate (99%), Sinopharm Chemical Reagent Co., Ltd.; *N,N*-diisopropylethylamine (99%), Sinopharm Chemical Reagent Co., Ltd.; dry dialysis bag (MWCO7000 Da), Yikang Trade Co., Ltd.; PBS solution (99%), Beijing Suolaibao Technology Co., Ltd.; CCK-8 solution, Biyuntian Biotechnology Co., Ltd.; lithium bromide (AR), Sinopharm Chemical Reagent Co., Ltd.; L929 cell, Zhejiang Meaysen Cell Technology Co., Ltd. The cell culture medium utilized during the experimental procedure was Dulbecco's modified Eagle's medium (DMEM), and fetal bovine serum (FBS), and trypsin-EDTA were procured from Gibco (USA). The entire operation was performed under a UV sterile bench, and all experimental personnel had undergone professional training. Macroscopic observation revealed that the cell culture medium remained clear, while microscopic examination under an electron microscope indicated no impurities around the cells, which exhibited favorable growth conditions. Furthermore, the cells have been validated for the absence of *Mycoplasma* contamination and authenticated by short tandem repeat (STR) profiling.

Synthesis process

Synthesis of double-bonded hyaluronic acid (HAMA)

According to literature [20], weigh 1.8 g of HA with a molecular weight of 100,000, fully dissolve it in 90 mL of deionized water, then add 60 mL of *N,N*-dimethylformamide (DMF) to it and mix well, then slowly add 2.88 mL of methacrylic anhydride water drop by drop, and react for 30 minutes. Then, a 1 mol/L sodium hydroxide aqueous solution was prepared, and the pH of the reaction solution was adjusted to 8–9 until the pH of the reaction solution was stable and no longer changed with time. After 24 hours of reaction, 0.9 g of sodium chloride was added and continued to react for half an hour. After the reaction was completed, the reaction solution was added to 360 mL of absolute ethanol solution, stirred to obtain a white precipitate, which was collected by centrifugation and dissolved in deionized water, dialyzed through a MWCO7000 dialysis bag for three days, and then freeze-dried to obtain double-bond modified hyaluronic acid (HAMA) [21] (Figure 1A).

Dopamine-modified double bond hyaluronic acid (HAC)

According to the literature [22], HAMA requires first conversion to the corresponding tetrabutylammonium salt (HAMA-TBA). Weigh 1.0 g of HAMA and completely dissolve it in 200 mL of deionized water, add 3.0 g of strong acidic cation exchange resin to react overnight, and then adjust the pH of the solution to 7.02–7.06 with tetrabutylammonium hydroxide (TBA-OH) to obtain an aqueous solution of HAMA-TBA, which is freeze-dried for later use. 1 mmol of freeze-dried HAMA-TBA was completely dissolved in 27 mL of deionized water, then 63 mL of DMF, 2.5 mmol of 1-hydroxybenzotriazole hydrate (HOBt), 2.5 mmol of *N,N*-diisopropylcarbodiimide (DIC) were added, and stirred evenly for 1 hour under the protection of nitrogen, then 2.5 mmol of dopamine hydrochloride, 0.5 mmol of 4-dimethylaminopyridine (DMAP) and 2.5 mmol of *N,N*-diisopropylethylamine (DIPEA) were added. The reaction was carried out under nitrogen protection at room temperature for 24 hours, and then the solution of the reaction was dialyzed using a dialysis bag with a molecular weight cut-off of 7,000 Da, in concentrated hydrochloric acid adjusted sodium chloride solution (1 M, pH = 5) for 1 day, followed by 4 days in deionized water. The dialyzed solution was lyophilized to obtain dopamine-modified double bonded hyaluronic acid (HAC). The route map for HAC synthesis (Figure 1B), the structure of the obtained HAC product was identified using ¹H-NMR, and the degree of substitution on it was calculated.

Preparation of amidated regenerated silk fibroin (SFMA)

Degumming: Weigh 30 g of chopped silkworm cocoons and boil them in a Na₂CO₃ aqueous solution with a concentration of 0.05 M, wash them with deionized water, and repeat the steps three times to remove the sericin remaining in the silk. Then, the degummed SF was completely dried in a constant temperature oven at 60°C to obtain SF fiber for later use.

Preparation of pure regenerated silk fibroin samples (RSF): Take 5 g of degummed SF fiber, fully dissolve it in 25 mL of 9.3 M LiBr aqueous solution in a water bath at 60°C, and put the dissolved aqueous solution into a dialysis bag (MWCO7000), dialyze it in deionized water for 3 days. After the dialysis is completed, centrifuge to remove insoluble impurities, and freeze dry the supernatant to obtain a pure regenerated SF powder sample with high purity.

Preparation of amidated regenerated silk fibroin (SFMA) [21]: According to the literature method [23], weigh 5 g of degummed SF fiber, place it into a 50 mL beaker, then add 25 mL of 9.3 M LiBr aqueous solution, stir in a constant temperature water bath at 60°C until the SF is completely dissolved, and then slowly add 2 mL of GMA to it to obtain a mixture with a GMA concentration of 604 mM. Under the condition of 300 rpm, stirring was continued for 3 hours to allow GMA and SF to completely react. The solution after the completion of the reaction was put into a dialysis bag (MWCO7000) and dialyzed in deionized water for 4 days. Finally, the dialyzed solution was centrifuged to remove impurities, and the supernatant was freeze-dried to obtain an SFMA powder sample (Figure 1C).

Preparation of hyaluronic acid/silk fibroin hydrogel (HASF) by rapid photo-curing

Dissolve methacrylated and dopamine-modified HA and methacrylated SF protein in deionized water, stir and mix well, and change the addition amount of SFMA (0%, 1%, 2%, 4%). By controlling the content of SF in the hydrogel, hyaluronic acid/silk fibroin hydrogel (HASF) gels with different degrees of crosslinking can be obtained. According to the feed ratio of hydrogel, it is used to formulate various HASF hydrogels (Table 1).

Table 1. Dosing ratios for HASF hydrogels

Sample	HAC (mg)	SFMA (mg)	H ₂ O (mL)	LAP (mg)
HAC-gel	60	0	1	1.5
HASF-gel-1	60	10	1	1.5
HASF-gel-2	60	20	1	1.5
HASF-gel-4	60	40	1	1.5

HAC: dopamine-modified double bonded hyaluronic acid; HASF: hyaluronic acid/silk fibroin hydrogel; SFMA: amidated regenerated silk fibroin

A series of hydrogel samples (HAC-gel, HASF-gel-1, HASF-gel-2, and HASF-gel-4) with varying degrees of crosslinking were prepared by adjusting the SFMA content.

Four groups of hydrogel photo-cured precursor fluids were prepared according to different feed ratios. LAP photo-initiator at a concentration of 0.001 g/mL was added to each group of solutions. After mixing evenly, precursor solutions of HAC-gel, HASF-gel-1, HASF-gel-2, and HASF-gel-4 were individually loaded into circular silicone molds with a diameter of 15 mm and a height of 4 mm. Photocuring was subsequently performed using a UV lamp (365 nm wavelength) operating at 18 W power output. The irradiation process was conducted for 30 seconds under controlled UV intensity set to 40 mW/cm².

Characterization

Nuclear magnetic resonance hydrogen spectroscopy (¹H-NMR)

¹H-NMR (Bruker AVANCE III 500MHz, Switzerland) was used to measure the ¹H-NMR spectra of HA before and after modification and SF before and after modification. Samples of HA, HAMA, HAC, RSF, and RSFMA were dissolved in D₂O at room temperature at a concentration of 10 mg/mL, and were characterized by ¹H nuclear magnetic resonance spectroscopy. MestReNova software was used to accurately calibrate our measurement data and calculate the degree of modification of different samples based on their corresponding integrated areas. The degree of modification of methacrylic anhydride (D_1) and dopamine (D_2) on the HA molecule is calculated according to Equations 1 and 2, respectively.

$$D_1(\%) = \left[\left(\frac{I_{6.10 \text{ ppm}} + I_{5.63 \text{ ppm}}}{2} \right) \div \left(\frac{I_{1.91 \text{ ppm}}}{3} \right) \right] \times 100\% \quad (1)$$

Among them, $I_{6.10 \text{ ppm}}$, $I_{5.63 \text{ ppm}}$, and $I_{1.91 \text{ ppm}}$ are the integrated areas of the signal peaks with chemical shifts at 6.10 ppm, 5.63 ppm, and 1.91 ppm.

$$D_2(\%) = \left(\frac{I_{6.5 \text{ ppm} \sim 7.0 \text{ ppm}}}{I_{3.0 \text{ ppm} \sim 4.0 \text{ ppm}}} \right) \times \frac{10}{3} \quad (2)$$

Among them, $I_{6.5 \text{ ppm} \sim 7.0 \text{ ppm}}$ is the area of the signal peak with chemical shifts of 6.5 ppm to 7.0 ppm, $I_{3.0 \text{ ppm} \sim 4.0 \text{ ppm}}$ is the area of the signal peak with chemical shifts of 3.0 ppm to 4.0 ppm, and the degree of substitution of vinyl groups on the SF molecule is calculated according to Equation 3.

$$D = \left(\frac{I_0 - I}{I_0} \right) \times 100\% \quad (3)$$

where D represents the degree of amidation on the SF molecule, and I_0 represents the integrated area of lysine in SF without GMA modification. I represent the integrated area of lysine in SFMA modified by GMA.

UV-Vis spectral

Prepare HAC and HAMA samples into aqueous solutions with a concentration of 1–2 mg/mL, pour them into 2/3 of the cuvette, and use a UV-Vis-NIR spectrometer (LAMBDA 750, PerkinElmer, USA) to perform absorption spectrum detection on the HAMA and HAC samples. Using deionized water as a control, scan the range of 100–600 nm, and measure the absorption peak.

Molecular weight determination

Gel permeation chromatography (GPC, Waters GPC 1515, USA) was used to measure the absolute molecular weight of HA before and after modification. Unmodified HA ($M_n = 100,000$), double-bonded modified HAMA and dopamine-modified double-bonded HAC were respectively prepared into aqueous solutions with a concentration of 3–6 mg/mL, and then the respective prepared solutions were passed through a chromatographic column to measure the absolute molecular weight.

Rheological properties

Rheological experiments were performed on the hydrogel samples using a rotary rheometer (Anton-Paar MCR 302, Austria), and they were analyzed. In the oscillation time sweep experiment, the changes of

storage modulus (G') and loss modulus (G'') with time were measured at a strain amplitude of 1% and a speed of 6.28 rad/s. The curing light source uses a 365 nm wavelength ultraviolet lamp with a power of 18 W, and the intensity of the ultraviolet lamp is set to 40.

Fourier transform infrared spectroscopy (FT-IR)

The changes in the molecular structure of amidated SF were analyzed by infrared spectroscopy (Nicolet iS50, Thermo Fisher, USA). The SFMA powder modified with GMA and the unmodified RSF powder were characterized in the range of 4,000–400 cm^{-1} .

Microscopic morphology of the hydrogels

The internal microstructure of the lyophilized hydrogel samples was observed using a benchtop scanning electron microscope (SEM, TESCAN VEGA3, Czech). The freeze-dried hydrogel samples HAC-gel, HASF-gel-1, HASF-gel-2, and HASF-gel-4 were brittle broken with liquid nitrogen, adhered to a standard cross-section table with conductive glue, and then the surface was sprayed with gold. The scanning voltage was set to 15 kV, and the magnification was adjusted to 50 times and 100 times to observe the internal morphology of the hydrogel.

Mechanical properties of hydrogels

The compression properties of the prepared hydrogels were measured using a high and low temperature dual column tester (Instron 5966, America). Precursors of HAC-gel, HASF-gel-1, HASF-gel-2, and HASF-gel-4 were placed in a silica gel orifice plate, and cylindrical samples with a diameter of about 15 mm and a height of about 4 mm were photocured to measure the compression properties of the hydrogels. The speed was set at 2 mm/min, and the compression shape variable was 80% until the hydrogel was broken and the experiment was stopped. Each group of samples was tested 3 times and the average value was taken.

Shear adhesion of hydrogel

Referring to the ASTM standard (F2255-05 method), the shear adhesion strength of the hydrogel was tested using a high and low temperature double column testing machine (Instron5966, USA) [24]. First, the fresh pig casings were cut into rectangular strips with a length of about 7 cm \times 2 cm. Secondly, the precursor liquids of HAC-gel, HASF-gel-1, HASF-gel-2, and HASF-gel-4 hydrogels were prepared, and the precursor liquids were evenly coated on the pig casings. One end was evenly coated and covered with another strip in the opposite direction. The coverage range of the prepared gel precursor liquid was about 4 cm^2 . Then, 365 nm ultraviolet light was irradiated for 30 seconds. After completing the bonding, the length b (cm) and the width l (cm) of the bonded part were measured. and record relevant data. Place the prepared specimen in the film fixture of a high-low-temperature double column testing machine, and stretch it at a speed of 5 mm/min with the long axis of the specimen as the force direction until the adhesive joint breaks, and obtain the maximum load of shear failure of the specimen— F (N). The shear adhesion strength τ (MPa) of the samples can be calculated from Equation 4, and the experiment is repeated three times for each group of samples.

$$\tau = \frac{F}{b \cdot l} \quad (4)$$

Biocompatibility

Swelling property

Hydrogels have the function of absorbing blood oozing from wounds, keeping wounds moist and accelerating healing. Therefore, it is necessary to evaluate their swelling characteristics. The swelling behavior of the prepared hydrogels was evaluated using a weighing method. Four groups of lyophilized hydrogel samples HAC-gel, HASF-gel-1, HASF-gel-2, and HASF-gel-4, were weighed respectively, the initial weight was recorded as W_0 (g), and the samples were immersed in 1 \times PBS solution at room temperature. After a fixed time, the swollen hydrogel was taken out, dried on a clean filter paper, weighed (W_t , g), and the swelling rate of the hydrogel was calculated by a formula.

The calculation formula for hydrogel swelling ratio is shown in [Equation 5](#):

$$\text{Swelling Ratio (\%)} = \frac{W_t - W_0}{W_0} \times 100\% \quad (5)$$

Degradation property

In vitro degradation experiments of HASF hydrogel were carried out with 1× PBS and 300 U/mL hyaluronidase solution. The dried HASF hydrogel column (diameter 15 mm, thickness 4 mm) was weighed. Place each component hydrogel in a 12-well plate, add 2 mL of PBS containing 300 U/mL to each well until it is completely immersed, and then place it in a constant temperature air bath at 37°C, and replace the PBS every two days. Take samples, freeze-dry, and weigh regularly to calculate the weight loss percentage of the initial hydrogel sample. The degradation rate calculation formula is as follows:

$$\text{Degradation Rate (\%)} = \frac{W_0 - W_d}{W_0} \times 100\% \quad (6)$$

where W_0 (g) is the initial dry weight of the HASF hydrogel, and W_d (g) is the dry weight of the hydrogel measured after a specific time.

Cell viability

The biocompatibility was evaluated by indirect contact method. Indirect contact method: L929 cells were seeded in a 24-well plate (5×10^4 cells) for 24 hours, and then treated with different concentrations of hydrogel soaking solution (hydrogel:DMEM, mass ratio 1:5) to treat for 24 hours. Add 10 μ L of CCK-8 solution to each well. After incubation for 2 hours, the absorbance was measured with a 450 nm microplate reader. Take A_s and A_c as the absorbance of the experimental and control groups, and A_b as the OD value of the blank group. The calculation formula is shown in [Equation 7](#).

$$\text{Cell Viability (\%)} = \frac{A_s - A_b}{A_c - A_b} \times 100\% \quad (7)$$

where A_s is OD_{experimental hole}, A_c is OD_{control hole}, and A_b is OD_{blank hole}.

For more biocompatibility experiments, please refer to the literature [\[25\]](#) of our group.

In vivo/vitro experiments

Animals

SD rats were approved by the Ethics Committee of Zhejiang Provincial People's Hospital (Ethics Permission No. 20230527175018933362). Diabetic male SD rats (250–300 g, $n = 6$) from Zhejiang Weitong Lihua Experimental Animal Technology Co., Ltd. were employed in this study. All animal care and experimental protocols were approved by the Animal Experimental Center of Zhejiang University of Technology and conducted in accordance with ethical guidelines. Following a one-week acclimatization period, the rats were anesthetized via intraperitoneal injection of pentobarbital sodium [\[26\]](#) (1%, 45 mg/kg), and their dorsal fur was shaved. Three circular wounds (1.2 cm in diameter) were created on the dorsal surface of each rat, with each wound receiving one of three treatments: HASF hydrogel precursor, Tegaderm (3M) dressing, or PBS. Wound healing was assessed at predefined time points, and wound size was quantified using ImageJ software. The day of surgery was designated as Day 0, and wounds were photographed and healing progress recorded on Days 1, 3, 5, and 10. On Day 7, the rats were humanely euthanized, and the wound tissue was harvested and fixed in 4% paraformaldehyde for paraffin embedding. Hematoxylin and eosin (H&E) and Masson's trichrome staining were performed by Xavier Biological Co., Ltd. 1% pentobarbital sodium was injected intraperitoneally at a dosage of 45 mg/kg body weight. After injection, the depth of anesthesia was monitored to ensure loss of consciousness and analgesia. Once adequately anesthetized, tissues or organs were collected according to the experimental protocol. All procedures were performed by trained personnel to ensure consistency and animal welfare. Following sample collection, euthanasia was performed by administering an additional dose of 1% pentobarbital sodium via intraperitoneal injection to ensure humane death without pain. The euthanasia of SD rats was performed via cervical dislocation, in accordance with standard protocols.

Hemostasis experiment

Hepatic hemorrhage models were established in 9 SD rats and its hemostatic effect in vivo was evaluated. First, anesthetics (1% sodium pentobarbital 45 mg/kg) were injected intraperitoneally, fixed on the operating table, and the abdomen of the rat was cut open to expose the liver. A 15 mm long and 5 mm deep incision was made on the liver of each mouse with a scalpel, and HASF hydrogel and commercially available gelatin sponge were immediately injected. The control group was not treated. Use a filter paper sheet to suck blood for 150 seconds. The change in weight before and after filtration with filter paper is the amount of wound bleeding (mg). The same method was used to repeat the measurements on different SD rats, and the average value was taken.

Construction and treatment of skin wound models

After one week of adaptive culture, SD rats ($n = 6$) were anesthetized by intraperitoneal injection with sodium pentobarbital (1% sodium pentobarbital 45 mg/kg) and their backs were depilated. We will construct and treat the wound model in accordance with the experimental procedures delineated in the aforementioned [Animals](#) section. HASF hydrogel precursor solution was applied to the wounds of rats and photocured to form gels. The wounds were treated with Tegaderm (3M) dressing and the wounds were treated with PBS. The wounds were observed at specific time points and photographed with a camera. The wound size was evaluated with ImageJ. The day of surgery was recorded as Day 1. Each treated wound was photographed on Days 1, 3, 5 and 10, and its healing status was recorded.

Wound histochemical staining

Rats were modeled and therapeutic interventions were given respectively according to the above method. On the 7th day, the rats were sacrificed, and the skin at the wound site was fixed in 4% paraformaldehyde, and paraffin sections were prepared for subsequent H&E staining, and the skin tissue was also stained with Masson. Both H&E staining and Masson staining were entrusted to Seville Biotech Co., Ltd.

Statistical analysis

All experimental results are presented as mean \pm standard deviation. Statistical comparisons were performed using one-way analysis of variance (ANOVA). The data were processed using GraphPad Prism 9.0 software, with Tukey's post hoc test yielding results consistent with our experimental findings. The significance thresholds were defined as follows: * $p < 0.05$ (statistically significant); ** $p < 0.01$ (highly significant); *** $p < 0.001$ (extremely significant); ns (not statistically significant).

Results

The preparation of hydrogels

Rapid photocuring preparation of HASF-gel

The photo-initiator LAP was added to the precursor liquid of the hydrogel, and the hydrogel sample HASF was successfully prepared under ultraviolet light irradiation. Hydrogel samples HAC-gel, HASF-gel-1, HASF-gel-2, and HASF-gel-4 with different crosslinking degrees were obtained by changing the content of SFMA. As the SFMA content increases, the transparency of the hydrogel decreases due to the increase in the degree of crosslinking of the HASF hydrogel and the changes in the internal structure of the hydrogel ([Figure 1K](#)).

The curing times of four groups of hydrogels were measured by the tilt method. The light curing times of the four groups of samples were 10 s, 12 s, 13 s, and 18 s, respectively, and all hydrogel groups were quickly cured and formed in tens of seconds. Shorter ultraviolet light irradiation can reduce toxic effects on cells and biological tissues.

In a word, all hydrogels rapidly gelled under the action of the initiator and UV light, with gelation times ranging from 10 to 20 s.

Characterization of HAC and SFMA precursors

To further confirm the successful modification of the SF molecule with GMA, we performed $^1\text{H-NMR}$ (Figure 1E) analysis on the modified SFMA. From the results, it can be seen that after GMA modification, two new NMR signal peaks appeared at two chemical shifts of 6.02 ppm and 5.60 ppm, respectively. They were caused by the vibration of two hydrogen nuclei in $\text{C}=\text{CH}_2$. An obvious methyl (CH_3) signal peak appeared at the chemical position of 1.8 ppm, and the vibration signal of the proton in $\text{N}-\text{CH}_2$ appeared at 3.30–3.70 ppm. In addition, it can be found from the spectrum that compared with pure SF, the signal peak intensity of lysine on the SF molecule modified with GMA is weaker. This may be due to the reaction of GMA with the lysine on the SF molecule, resulting in the decrease in the content of lysine, and the spectrum shows that the signal peak intensity of lysine becomes weaker. At the same time, the GMA modification degree was calculated to be 34.8% through quantitative analysis of nuclear magnetic resonance spectra. Combined with FT-IR characterization results, it was confirmed that GMA could effectively amidate SF.

Comparing the nuclear magnetic spectra of HA and HAMA (Figure 1D), it was observed that three new signal peaks appeared on the HAMA spectrum, one partial peak at about 1.84 ppm, and two new nuclear magnetic peaks at 6.1 ppm and 5.63 ppm. These three peaks are all characteristic peaks of MA, which are signal peaks of methyl hydrogen of MA and two hydrogen atoms on the double bond carbon. The integrated area of MA hydrogen was compared with the integrated area of HA methyl hydrogen. The modification degree of MA on HA was calculated to be 47%. Comparing the nuclear magnetic spectra of HAMA and HAC, it can be found that a new peak at 6.5–7.0 ppm has been added to the spectra of HAC. These three chemical shift peaks correspond to the chemical shift values of hydrogen on the three carbons at positions 2, 3 and 4 on the dopamine benzene ring, respectively, indicating that dopamine hydrochloride has been successfully modified onto methacrylic acid liver modified HA. The peak of 3.0–4.0 ppm indicates the signal peak presented by hydrogen atoms on the two six-membered ring skeletons of HA. The degree of substitution of dopamine calculated from the peak area is about 34.6%, which is close to that reported in the document [22].

Infrared spectrum analysis of SFMA (Figure 1F) was carried out using FT-IR to initially judge the modification effect of GMA on SF. The GMA and SF-related peaks were identified from the spectra, and the relationship between the two was confirmed. The spectra of RSF and GMA modified SFMA samples both showed that the peaks of amide type I, type II and type III were located at 1,639, 1,517 and 1,234 cm^{-1} , respectively. From the spectrum, we can find that SFMA has a new peak with a weak band at a wave number of 1,295 cm^{-1} , which may be related to the stretching vibration of the alcoholic hydroxyl group ($-\text{CHOH}$) generated after the ring-opening reaction between the epoxy group on GMA and the SF molecule. In addition, weak peaks appeared at wavenumbers of approximately 950 cm^{-1} and 1,120 cm^{-1} , representing the stretching vibration of the methacrylate vinyl group ($-\text{C}=\text{CH}_2$) in GMA. This peak is not obvious in the spectrum, probably because it is covered by the peak positions of other structures. In addition, since the molecular weight of GMA is much smaller than SF, the GMA functional groups can only be slightly detected or hidden.

Generally speaking, in the UV-visible spectrum, the catechol group has a typical absorption peak at 280 nm (assigned to the $\pi-\pi^*$ absorption band). By absorbance measurement of HAMA and HAC solutions (Figure 1G), the single absorption peak of HAC appears at 280 nm, and no obvious absorption peak is observed in HAMA, indicating that the dopamine catechol structure has been successfully grafted to HAMA, and there are no other peaks at wavelengths greater than 300 nm, indicating that the catechol conjugated structure has not been oxidized.

GPC testing was performed on the synthesized HAC and HAMA, and the results showed that (Figure 1H), the weight-average molecular weight M_w of HAC is 2.4×10^5 g/mol, the number-average molecular weight M_n is 1.46×10^5 g/mol, and the molecular weight distribution coefficient (PDI) is 1.656. The weight-average molecular weight M_w of HAMA is 1.8×10^5 g/mol. The number-average molecular weight M_n is 1.1×10^5 g/mol and the molecular weight distribution coefficient (PDI) is 1.653. The weight-average molecular weight M_w of raw material HA-10W is 1×10^4 g/mol. The number average molecular

weight M_n is 1.4×10^5 g/mol, and the distribution coefficient (PDI) is 1.45. As shown in [Figure 1H](#), the molecular weight of the modified HA becomes larger.

The crosslinking and the structure of hydrogels

The changes in storage modulus G' and loss modulus G'' of copolymer hydrogels with different content ratios were studied by rheological methods ([Figure 1I](#)). When the elastic modulus is greater than the viscosity modulus, the hydrogel is in a gel state and is first scanned for time under ultraviolet radiation from a rheometer. All hydrogel precursors are stabilized for 25 s before turning on the ultraviolet light source to irradiate. All solutions have stable G' and G'' before ultraviolet light irradiation. When the ultraviolet lamp is turned on, G' increases rapidly as the illumination time increases, then exceeds G'' , and finally reaches a plateau within 300 s. We found that the addition of SFMA had a certain impact on the gel point time (the G' and G'' data curves crossed). When the addition of SFMA was 4%, the longest gel point time was about 22 s, indicating that the hydrogel precursor requires more time to crosslink.

By controlling the SFMA content, the degree of crosslinking in the hydrogels could be adjusted, resulting in porous network structures with different crosslinking densities. Mechanical, swelling, and degradation tests confirmed that the properties of the hydrogels were directly influenced by their crosslinking density.

The internal structure of hydrogels plays a key role in the performance of materials. Therefore, the internal microstructures of four groups of hydrogel samples HAC-gel, HASF-gel-1, HASF-gel-2, and HASF-gel-4 were observed through a benchtop scanning electron microscope ([Figure 1J](#)). It can be seen from the figure that all components of hydrogels have interconnected and uniform porous microstructures, and the internal cross-linked structure of hydrogels remains intact after freeze-drying. The pores of HAC/SFMA composite gels of different components penetrate through to form a unique 3D porous structure, which is conducive to the transport of oxygen and nutrients, and also creates conditions for cell growth. In addition, with the increase of SFMA concentration, the pore size of the hydrogel slightly increases, which is due to the increase in cross-linking degree of HASF hydrogel and changes in the internal structure of the hydrogel. This unique loose porous structure provides an ideal growth environment for cells. These pores not only facilitate tight adhesion between cells but also promote their migration and distribution. At the same time, this material can maintain a moist microenvironment, which is crucial for the absorption of exudate from the wound. Due to the existence of these holes, new tissue can adapt to the surrounding environment more quickly, thus accelerating the process of wound healing. In addition, the porosity of this structure also allows liquids and nutrients to flow inside the material, further enhancing the support and nourishment of damaged areas [[27](#), [28](#)].

Mechanical and adhesive properties of hydrogels

Effective hemostatic materials should have sufficient mechanical strength to protect wounds and promote tissue healing. We conducted mechanical compression tests on hydrogel samples HAC-gel, HASF-gel-1, HASF-gel-2, and HASF-gel-4, and measured the compressive strain (%) on the X-axis and the compressive stress on the Y-axis (MPa), where HAC is a hydrogel without SFMA added, and the compressive strengths of the four groups of hydrogels are 0.22 MPa, 0.25 MPa, 0.33 MPa, and 0.44 MPa, respectively, indicating that with the increase of SFMA content, the compressive strength of the hydrogel is improved to a certain extent, and the degree of crosslinking of the hydrogel increases ([Figure 2A](#)). In addition, the four groups of hydrogel samples fractured at compressive strains of 42.85%, 50.28%, 49.51%, and 50.71%, respectively, indicating that changes in SFMA content can improve the toughness of the hydrogel to a certain extent, and the adjustable compressive strength of the hydrogel can be better applied to various tissues.

The good tissue adhesion of hydrogels can promote wound sealing to stop bleeding, create a physical barrier to prevent bacterial invasion, promote cell growth and differentiation, and provide a moist environment to accelerate wound healing. To this end, we investigated the adhesion properties of the prepared hydrogels. We used pig casings as skin tissue to study the adhesion strength of the hydrogel through lap shear tests ([Figure 2B](#)). As shown in [Figures 2C](#) and [2D](#), the prepared hydrogel HASF-gel-2 has

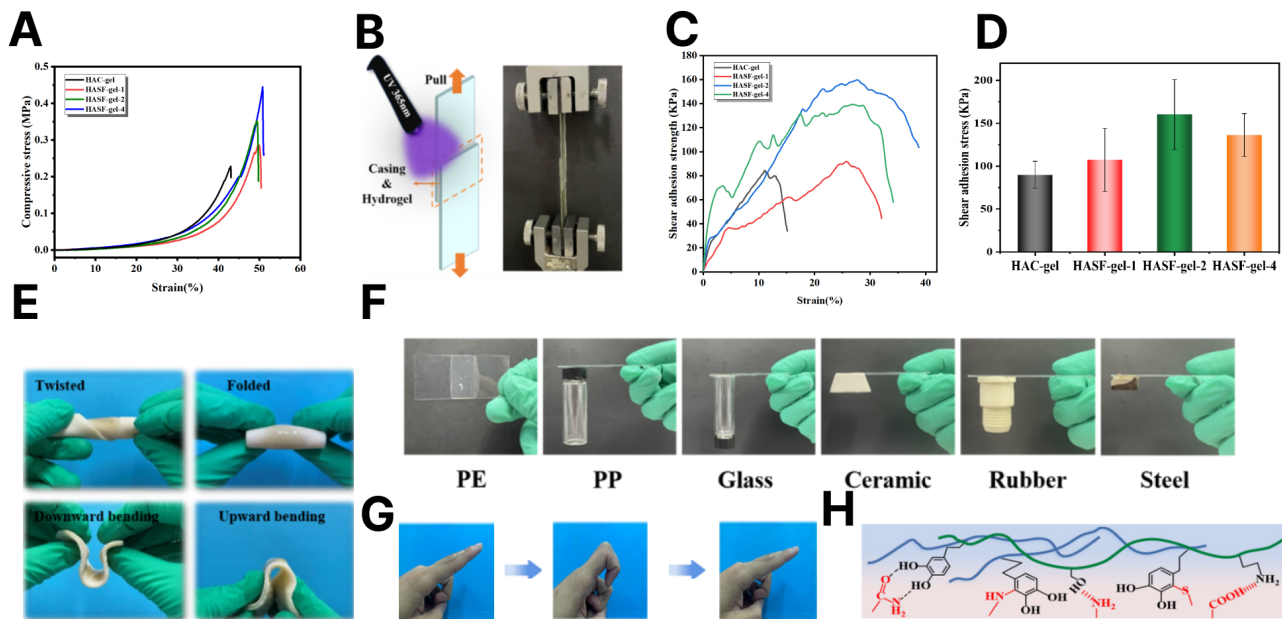


Figure 2. Property of hydrogel. **A)** Compression performance of hydrogel samples. **B)** Schematic diagram and photos of hydrogel lap shear test. **C)** Shear tensile curves of hydrogels with different SFMA contents on wet pig casings. **D)** Shear adhesion strength of hydrogels with different SFMA contents on pig casing substrate. **E)–G)** Schematic diagram of hydrogel adhesion to human finger joints, pig skin surface and other different substrates. **H)** Hydrogel adhesion mechanism. HAC: dopamine-modified double bonded hyaluronic acid; HASF: hyaluronic acid/silk fibroin hydrogel

a maximum adhesion strength of 160.3 kPa, while the adhesion strengths of HAC-gel, HASF-gel-1, and HASF-gel-4 are 71.96 kPa, 117.35 kPa, and 136.51 kPa, respectively. Adding a suitable amount of SFMA can further improve the adhesion strength of the hydrogel, and the reduction of the adhesion performance of HASF-gel-4 may be related to the crosslinking density of the hydrogel. Comparison found that the adhesive strength of the prepared HASF hydrogel was much higher than that of the marketed fibrin glue (2–40 kPa). **Figures 2E** and **2G** show that the prepared hydrogel HASF-gel-2 not only has good adhesion to human finger joints, but also has excellent adhesion flexibility to fresh pig skin and will not separate when stretched, bent, rolled and twisted. In addition, we also found that the prepared hydrogel HASF-gel-2 can also be easily cured in situ and adhered to various materials, as shown in **Figure 2F**. All of the good adhesion properties of the hydrogel are attributed to the dopamine catechol structure grafted on HA and some functional groups, such as amino groups on SF that interact with the tissue interface to produce adhesion (**Figure 2H**). This adhesion effect allows the hydrogel to maintain good adhesion properties even in a humid environment.

All hydrogels exhibited strong adhesion, and the addition of SFMA improved their adhesive properties. The hydrogels adhered well to various surfaces and were capable of adapting to shape changes without breaking or peeling, showing promise for use as wound dressings.

Biocompatibility

Swelling properties

In a liquid environment, hydrogels will swell to varying degrees, and a suitable swelling rate is the key to maintaining their good structure. In order to investigate the swelling behavior of the prepared hydrogels, hydrogel swelling tests were carried out on four groups of hydrogel samples of HAC-gel, HASF-gel-1, HASF-gel-2, and HASF-gel-4 in 1× PBS solution. The swelling behavior and equilibrium swelling of each group of hydrogel samples. As shown in **Figures 3A** and **3B**, all hydrogels showed the ability to absorb water rapidly in the first 1 hour, and could reach an equilibrium swelling state within 4 hours. A stable swelling rate could be maintained for a period of time. This shows that the hydrogel has relatively good size stability, and good swelling properties are conducive to the adsorption of wound exudate by the hydrogel wound dressing. HAC-gel has the highest swelling ratio of 2,100%, and the HASF-gel-4 hydrogel sample has the lowest swelling ratio of 1,288%. The swelling ratio of HASF hydrogel decreases with the increase of SFMA concentration. The addition of SFMA results in the formation of hydrogels with a higher degree of crosslinking, so the equilibrium swelling ratio of the hydrogels is lower.

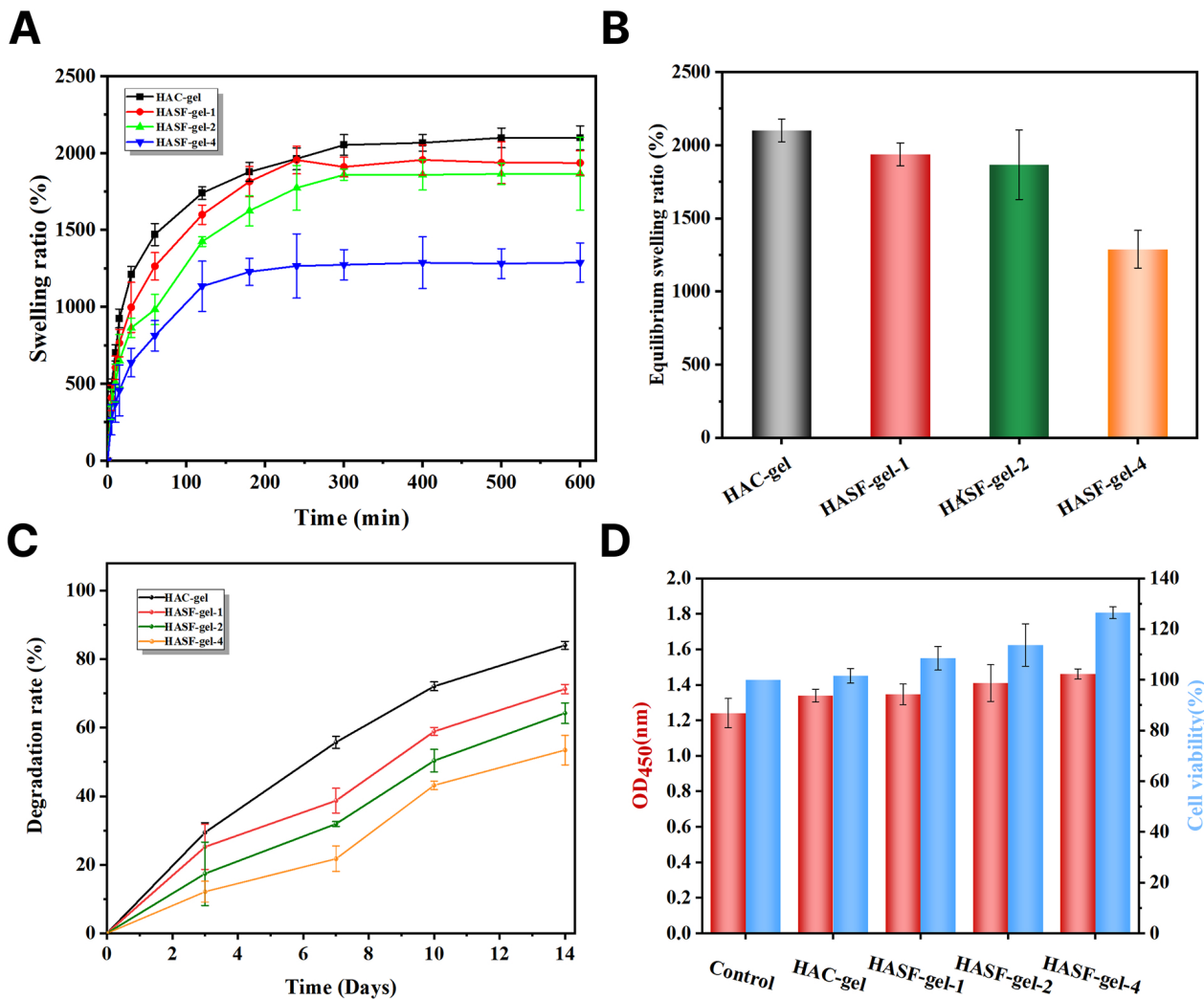


Figure 3. Biocompatibility properties of hydrogel. A) Swelling behavior of HASF hydrogels in PBS buffer. B) Equilibrium swelling ratio of HASF hydrogels in PBS buffer. C) Degradation behavior of HASF hydrogel. D) OD and cell viability of HASF hydrogel after 24 h of L929 cell culture. HAC: dopamine-modified double bonded hyaluronic acid; HASF: hyaluronic acid/silk fibroin hydrogel

Degradation property

The degradation behavior of materials plays a crucial role in many applications of tissue engineering. It not only affects the stability and long-term performance of biological scaffolds or tissue substitutes, but also affects the treatment effect and patient satisfaction. Under ideal conditions, the degradation rate of hydrogel should maintain a quick-fitting relationship with the growth of tissue and skin. To this end, we explored the in vitro degradation behavior of the prepared hydrogel. In vitro degradation curves of the hydrogels obtained by placing hydrogel samples of HAC-gel, HASF-gel-1, HASF-gel-2, and HASF-gel-4 in PBS solution containing hyaluronidase for 2 weeks (Figure 3C). It can be seen from the figure that the degradation rates of HAC-gel, HASF-gel-1, HASF-gel-2, and HASF-gel-4 hydrogels decrease in turn over time. All hydrogel groups could degrade by 80% within two weeks, and HASF-gel-4 hydrogel degrades relatively slowly than the pure HAC-gel group. This is attributed to the relatively high degree of crosslinking of HASF-gel-4 hydrogel. The degradation rate of hydrogel can be changed by adjusting the content of SFMA.

Cell viability

The biocompatibility of HAC-gel, HASF-gel-1, HASF-gel-2, and HASF-gel-4 hydrogel samples was characterized by the CCK-8 kit [25] (Figure 3D). WST-8 in the kit was reduced to a highly water-soluble yellow formazan product by the dehydrogenase in the cells under the action of the electron carrier. The amount of formazan produced is proportional to the number of living cells. Therefore, this characteristic can be used to directly conduct cell proliferation and toxicity analysis. The optimal measurement time can

be selected for multiple determinations. Compared with the MTT method, the linear range is wider and the sensitivity is higher.

The cell viability value of the control group was 1, and the cell viability values of HAC-gel, HASF-gel-1, HASF-gel-2, and HASF-gel-4 hydrogels were 1.015, 1.085, 1.136, and 1.263, respectively, which were higher than the control group, indicating that the prepared hydrogel group has good biocompatibility, and the addition of appropriate amount of silk protein is conducive to cell proliferation and provides a good growth environment for cell culture.

Biocompatibility tests indicated that all hydrogels had good biocompatibility, with the hydrogel groups promoting cell proliferation compared to the control group.

Hemostatic property

The first process of wound treatment is that the material can quickly stop bleeding. To this end, we evaluated the hemostatic performance of the hydrogel through an SD rat liver injury model. Combined with hydrogel formation time, mechanical properties, and adhesion properties, we selected HASF-gel-2 hydrogel group samples for animal experiments. Figures 4A and 4B are schematic diagrams of hemostasis of liver injury in SD rats. The average hemostasis time in the HASF-gel-2 hydrogel group was 15 s, which was significantly shorter than that in the negative control group (110 s, $p < 0.001$) and shorter than that in the sponge group (47 s, $p < 0.05$) (Figure 4C).

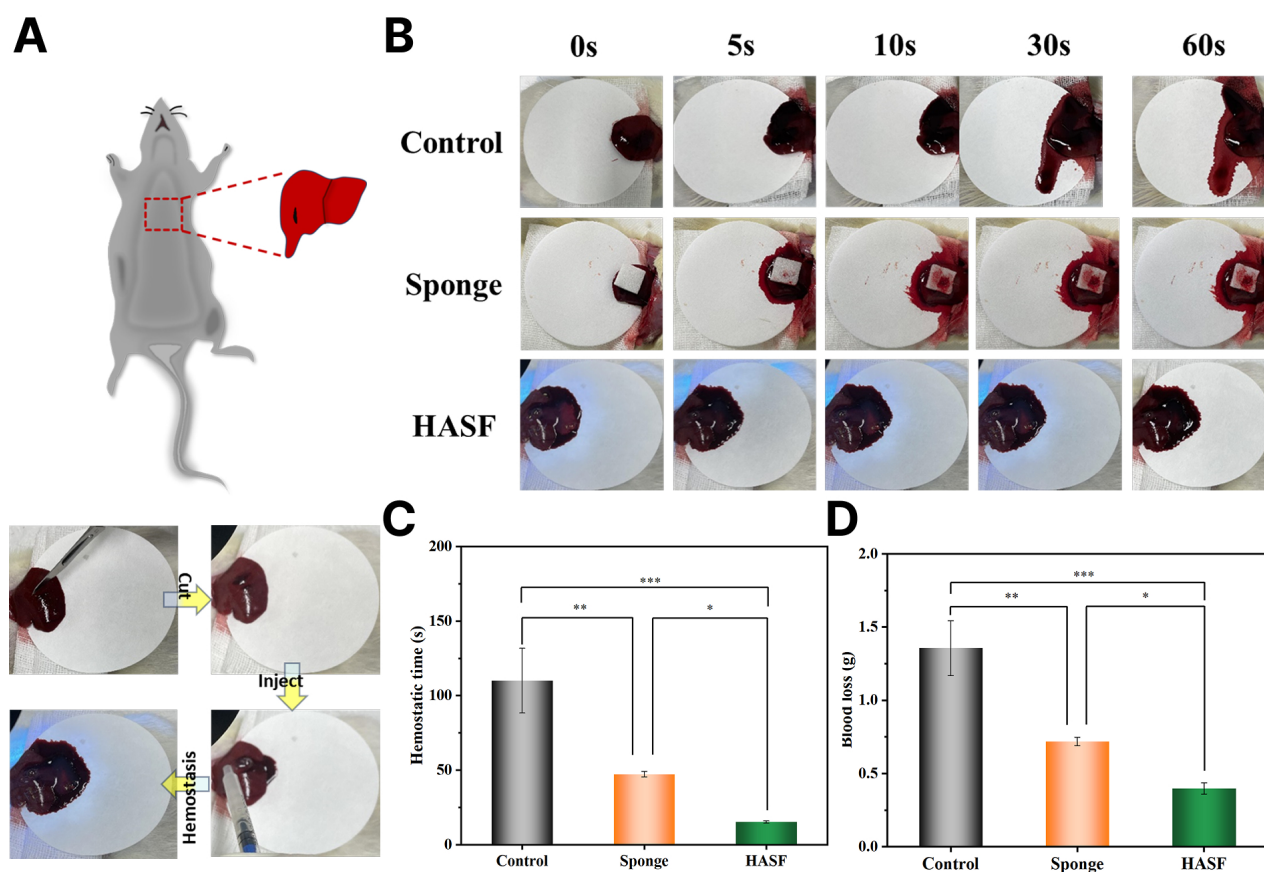


Figure 4. Hemostatic properties of hydrogels (HASF-gel-2). A) & B) Schematic diagram of hemostasis of liver injury in SD rats. C) Hemostasis time. D) Hemostasis amount. * $p < 0.05$; ** $p < 0.01$; *** $p < 0.001$. HASF: hyaluronic acid/silk fibroin hydrogel

At the same time, the average blood loss in the HASF-gel-2 hydrogel group was 0.415 g, which was significantly smaller than that in the negative control group (1.49 g, $p < 0.001$) and smaller than that in the sponge group (0.71 g, $p < 0.05$) (Figure 4D). The above results show that the hydrogel can have a good hemostatic effect on liver injury and can quickly stop bleeding. The good hemostatic properties of HASF-

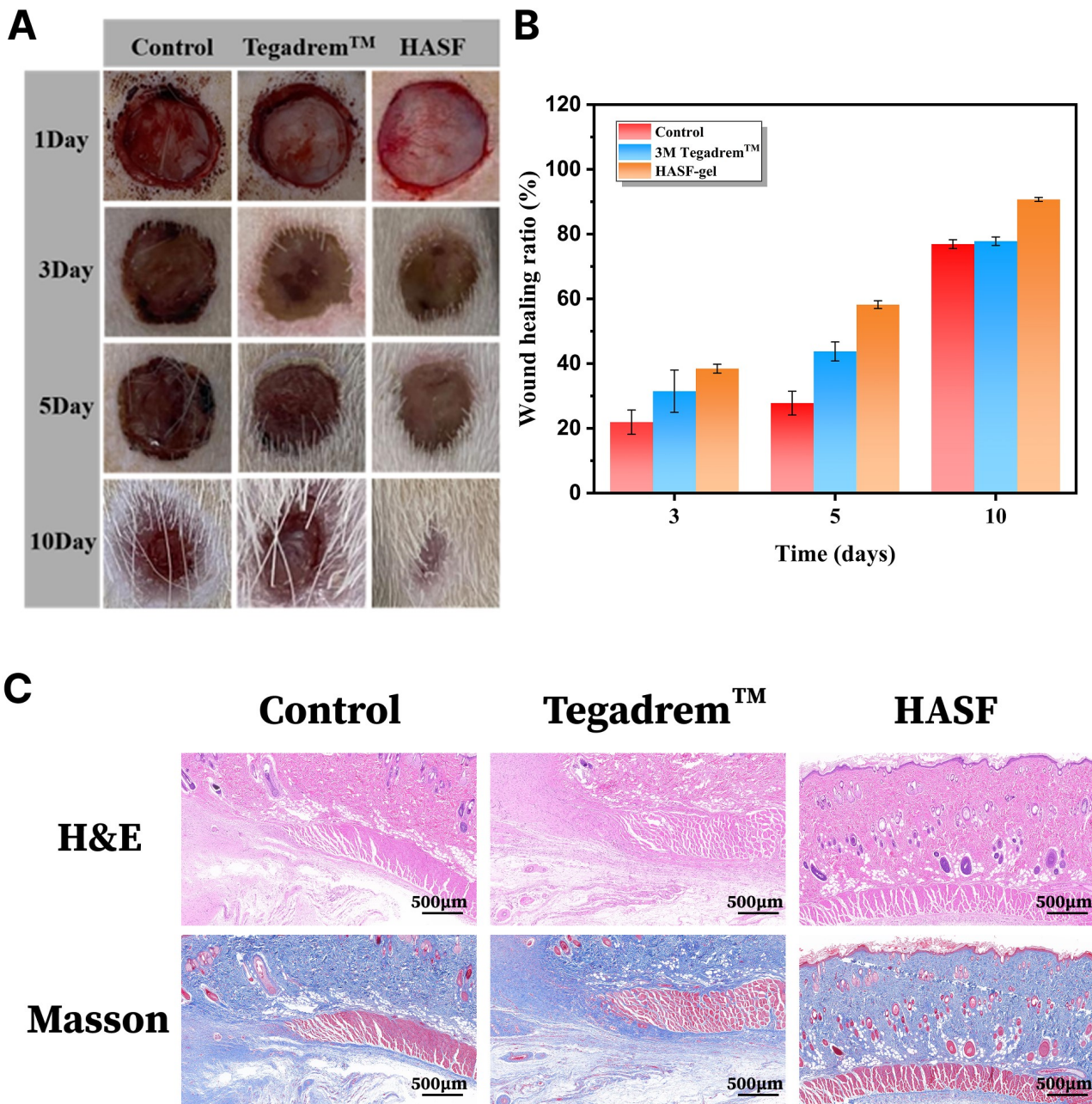


Figure 5. Wound healing and histopathological images of wound tissue. A) Representative image of wound healing. **B)** Statistics of wound healing rate. **C)** Representative image of wound tissue with H&E and Masson staining. HASF: hyaluronic acid/silk fibroin hydrogel

gel-2 hydrogel are mainly attributed to the close adhesion between the hydrogel formed in situ and the tissue. Good hemostasis is the key to promoting wound healing.

In vivo wound healing experiments in SD rats showed that HASF-gel-2 exhibited excellent hemostatic properties and significantly promoted wound healing.

Wound healing

The above experiments show that HASF hydrogel has good mechanical properties, tissue adhesion properties, good biocompatibility and potential ability to promote cell proliferation. Therefore, we speculate that HASF hydrogel can promote wound healing. To this end, we evaluated the therapeutic effect of HASF hydrogel on wound wounds in SD rats. As shown in [Figure 5A](#), on the first day of initial wound formation, the initial wound sizes of the three groups were basically the same. On the third day, the blank control group had no significant shrinkage. Wounds in the HASF hydrogel (41.7%) and 3M dressing groups

(38.6%) began to shrink and heal (Figure 5B). On the fifth day, the wounds in the three groups began to scab, among which the hydrogel group healed best. By the tenth day, the wounds in the hydrogel group had almost closed, and the treatment effect was better than that in the commercial 3M dressing group and the control group.

In order to further evaluate the healing of the wound, the rat wounds and surrounding tissues on Day 10 were removed for H&E and Masson staining analysis. The results are shown in Figure 5C. It can be seen from the figure that the HASF hydrogel epidermis has been regenerated and the epidermis is closest to the thickness of normal skin. During the process of wound healing, granulation tissue plays an important role in absorbing necrotic tissue and protecting the wound. Therefore, the thickness of granulation tissue can evaluate the progress of wound healing. It can be seen from the figure that the granulation tissue in the control group and 3M dressing group did not completely fill the wound surface and most of the tissue grew immature, while the granulation tissue of HASF hydrogel grew well and most of the granulation tissue filled the wound surface, with a significant treatment effect. This indicates that the wound tissue sections in the HASF hydrogel group showed a faster healing effect. In addition, Masson staining was performed on different groups to reflect collagen deposition. Collagen deposition is a major component of the skin and plays a key role in wound healing. As the collagen content in the wound increases significantly, the regenerative ability of cells has been enhanced unprecedentedly. This nutrient plays a key role in promoting tissue repair, accelerating the process of wound healing, and allowing damaged areas to recover quickly. In the HASF hydrogel group, it can be found that the collagen area at the wound is larger and the collagen fibers are denser, which has a good wound repair effect.

Discussion

Through methacrylation modification of HA and dopamine-grafting functionalization of SF, photo-crosslinkable HASF hydrogels were synthesized via rapid ultraviolet-initiated polymerization. By modulating the SFMA (methacrylated SF) concentration, hydrogels with graded crosslinking densities—designated as HAC-gel, HASF-gel-1, HASF-gel-2, and HASF-gel-4—were fabricated. Structural characterization via SEM micrographs revealed uniformly porous architectures across all variants, with a positive correlation between SFMA content and pore diameter enlargement. Compressive mechanical testing demonstrated that the crosslinking density, governed by SFMA dosage, directly dictated the hydrogel's mechanical robustness, exhibiting enhanced compressive modulus and fracture resistance with increasing SFMA incorporation.

Swelling and degradation assays further validated the tunable crosslinking-dependent hydrogel stability. Lap-shear adhesion testing indicated optimal interfacial bonding strength when SFMA was incorporated at intermediate concentrations, achieving tissue-adhesive performance compatible with physiological substrates. In vivo evaluations substantiated the hydrogel's exceptional hemostatic efficacy, achieving rapid hemorrhage control within 20 s in murine hemorrhage models. Furthermore, full-thickness dermal wound experiments in rats demonstrated accelerated epithelialization and collagen deposition in HASF hydrogel-treated groups, confirming its pro-regenerative capacity.

Conclusions

HA exhibits excellent biocompatibility, degradability, and moisture retention, and plays a key role in inflammation, angiogenesis, and tissue regeneration. SF is known for its low immunogenicity, good biocompatibility, degradability, and exceptional mechanical properties, along with water and oxygen permeability. SF-based hydrogels show great potential in the repair of skin, blood vessels, and other tissues. Through methacrylation and dopamine grafting modifications, HA and SF can be photo-crosslinked under the action of an initiator to form HASF hydrogel. Due to their rapid gelation and in-situ polymerization, photo-crosslinked hydrogels have gained wide application in skin wound treatment.

As an adhesive and antibacterial dressing, HASF hydrogel holds promise for drug and bioactive factor delivery, with broad potential applications in wound repair.

Abbreviations

DMEM: Dulbecco's modified Eagle's medium

DMF: *N,N*-dimethylformamide

FT-IR: Fourier transform infrared spectroscopy

GMA: glycidyl methacrylate

GPC: gel permeation chromatography

H&E: hematoxylin and eosin

HA: hyaluronic acid

HAC: dopamine-modified double bonded hyaluronic acid

HAMA: double-bond modified hyaluronic acid

HASF: hyaluronic acid/silk fibroin hydrogel

MA: methacrylate anhydride

RSF: regenerated silk fibroin

SF: silk fibroin

SFMA: amidated regenerated silk fibroin

TBA: tetrabutylammonium

Declarations

Author contributions

SL: Investigation, Writing—original draft, Writing—review & editing, Project administration. WP: Resources, Funding acquisition. MC: Investigation, Validation, Writing—review & editing. RW: Validation, Writing—review & editing. FC: Formal analysis, Methodology, Writing—review & editing.

Conflicts of interest

Feng Chen who is the Editorial Board Member and Guest Editor of *Exploration of BioMat-X* had no involvement in the decision-making or the review process of this manuscript. The other authors declare that they have no conflicts of interest.

Ethical approval

All animal procedures were conducted in accordance with the People's Republic of China Animal Protection Law and relevant regulations. The experimental protocol was approved by the Zhejiang Provincial People's Hospital Animal Ethics Committee, approval number 20230527175018933362. The experiments shown in subfigures E–G of Figure 2, involving fingers, were designed to visually and intuitively demonstrate the hydrogel's adhesion to the skin surface. This does not involve formal human subject experiments and is a commonly used illustrative method in hydrogel studies; therefore, ethical approval is not required.

Consent to participate

As stated in Ethical approval, informed consent is not required.

Consent to publication

Not applicable.

Availability of data and materials

The raw data supporting the conclusions of this manuscript will be made available by the authors, without undue reservation, to any qualified researcher.

Funding

This study was supported by Zhejiang Province Leading Soldier and Goose Program [2024C03094]. The funders had no role in study design, data collection and analysis, decision to publish, or preparation of the manuscript.

Copyright

© The Author(s) 2025.

Publisher's note

Open Exploration maintains a neutral stance on jurisdictional claims in published institutional affiliations and maps. All opinions expressed in this article are the personal views of the author(s) and do not represent the stance of the editorial team or the publisher.

References

1. Farahani M, Shafiee A. Wound Healing: From Passive to Smart Dressings. *Adv Healthc Mater.* 2021;10:e2100477. [DOI] [PubMed]
2. Li J, Li Y, Guo C, Wu X. Development of quercetin loaded silk fibroin/soybean protein isolate hydrogels for burn wound healing. *Chem Eng J.* 2024;481:148458. [DOI]
3. Chen G, Wang F, Zhang X, Shang Y, Zhao Y. Living microecological hydrogels for wound healing. *Sci Adv.* 2023;9:eadg3478. [DOI] [PubMed] [PMC]
4. Yu Y, Yang B, Tian D, Liu J, Yu A, Wan Y. Thiolated hyaluronic acid/silk fibroin dual-network hydrogel incorporated with bioglass nanoparticles for wound healing. *Carbohydr Polym.* 2022;288:119334. [DOI] [PubMed]
5. Yang Y, Zhong S, Meng F, Cui X. Multi-Functional hydrogels to promote diabetic wound healing: A review. *Chem Eng J.* 2024;497:154855. [DOI]
6. Chin JS, Madden L, Chew SY, Becker DL. Drug therapies and delivery mechanisms to treat perturbed skin wound healing. *Adv Drug Deliv Rev.* 2019;149–150:2–18. [DOI] [PubMed]
7. Bombin ADJ, Dunne NJ, McCarthy HO. Electrospinning of natural polymers for the production of nanofibres for wound healing applications. *Mater Sci Eng C Mater Biol Appl.* 2020;114:110994. [DOI] [PubMed]
8. Zare I, Chevrier DM, Cifuentes-Rius A, Moradi N, Xianyu Y, Ghosh S, et al. Protein-protected metal nanoclusters as diagnostic and therapeutic platforms for biomedical applications. *Mater Today.* 2023;66:159–93. [DOI]
9. Zhou L, Xu P, Dong P, Ou X, Du X, Chen Y, et al. A self-pumping dressing with in situ modification of non-woven fabric for promoting diabetic wound healing. *Chem Eng J.* 2023;457:141108. [DOI]
10. Wang L, Zhou M, Xu T, Zhang X. Multifunctional hydrogel as wound dressing for intelligent wound monitoring. *Chem Eng J.* 2022;433:134625. [DOI]
11. Wang H, Zhang LM. Intelligent biobased hydrogels for diabetic wound healing: A review. *Chem Eng J.* 2024;484:149493. [DOI]
12. Qi C, Sun Q, Xiao D, Zhang M, Gao S, Guo B, et al. Tetrahedral framework nucleic acids/hyaluronic acid-methacrylic anhydride hybrid hydrogel with antimicrobial and anti-inflammatory properties for infected wound healing. *Int J Oral Sci.* 2024;16:30. [DOI] [PubMed] [PMC]
13. Li Y, Han Y, Li H, Niu X, Zhang D, Wang K. Antimicrobial Hydrogels: Potential Materials for Medical Application. *Small.* 2023;20:2304047. [DOI]
14. Khosravimelal S, Mobaraki M, Eftekhari S, Ahearne M, Seifalian AM, Gholipourmalekabadi M. Hydrogels as Emerging Materials for Cornea Wound Healing. *Small.* 2021;17:e2006335. [DOI] [PubMed]
15. Graça MFP, Miguel SP, Cabral CSD, Correia IJ. Hyaluronic acid-Based wound dressings: A review. *Carbohydr Polym.* 2020;241:116364. [DOI] [PubMed]

16. Fraser JR, Laurent TC, Laurent UB. Hyaluronan: its nature, distribution, functions and turnover. *J Intern Med.* 1997;242:27–33. [DOI] [PubMed]
17. Toole BP. Hyaluronan in morphogenesis. *Semin Cell Dev Biol.* 2001;12:79–87. [DOI] [PubMed]
18. Lin D, Li M, Wang L, Cheng J, Yang Y, Wang H, et al. Multifunctional Hydrogel Based on Silk Fibroin Promotes Tissue Repair and Regeneration. *Adv Funct Mater.* 2024;34:2405255. [DOI]
19. Yu R, Yang Y, He J, Li M, Guo B. Novel supramolecular self-healing silk fibroin-based hydrogel via host–guest interaction as wound dressing to enhance wound healing. *Chem Eng J.* 2021;417:128278. [DOI]
20. Zhang Q, Wei X, Ji Y, Yin L, Dong Z, Chen F, et al. Adjustable and ultrafast light-cured hyaluronic acid hydrogel: promoting biocompatibility and cell growth. *J Mater Chem B.* 2020;8:5441–50. [DOI] [PubMed]
21. Chen L, Zhong M, Chen J, Liu Z, Kuang T, Liu T, et al. Preparation of silk fibroin/hyaluronic acid composite hydrogel based on thiol-ene click chemistry. *Zhejiang Da Xue Xue Bao Yi Xue Ban.* 2023;52:285–95. [DOI] [PubMed] [PMC]
22. Zhang K, Wei Z, Xu X, Feng Q, Xu J, Bian L. Efficient catechol functionalization of biopolymeric hydrogels for effective multiscale bioadhesion. *Mater Sci Eng C Mater Biol Appl.* 2019;103:109835. [DOI] [PubMed]
23. Rockwood DN, Preda RC, Yücel T, Wang X, Lovett ML, Kaplan DL. Materials fabrication from *Bombyx mori* silk fibroin. *Nat Protoc.* 2011;6:1612–31. [DOI] [PubMed] [PMC]
24. Qiao Z, Lv X, He S, Bai S, Liu X, Hou L, et al. A mussel-inspired supramolecular hydrogel with robust tissue anchor for rapid hemostasis of arterial and visceral bleedings. *Bioact Mater.* 2021;6:2829–40. [DOI] [PubMed] [PMC]
25. Yang F, Chen Y, Zhang W, Gu S, Liu Z, Chen M, et al. Tunable and fast-cured hyaluronic acid hydrogel inspired on catechol architecture for enhanced adhesion property. *Int J Biol Macromol.* 2024;271:132119. [DOI] [PubMed]
26. Chen D, Yang X, Jiang X, Li H, Jing B. Clinical and Experimental Study of effects of rhubarb on gastrointestinal blood flow perfusion in critical illness. *Chin J Integr Tradit West Med.* 2001;7:2–6. [DOI]
27. Jiang S, Lyu C, Zhao P, Li W, Kong W, Huang C, et al. Cryoprotectant enables structural control of porous scaffolds for exploration of cellular mechano-responsiveness in 3D. *Nat Commun.* 2019;10:3491. [DOI]
28. Huang Q, Zou Y, Arno MC, Chen S, Wang T, Gao J, et al. Hydrogel scaffolds for differentiation of adipose-derived stem cells. *Chem Soc Rev.* 2017;46:6255–75. [DOI] [PubMed]